Eigenmodes and Green's function of swirling flow in a duct with the lining varying circumferentially

James R. Mathews* and N Peake†

University of Cambridge, Cambridge, CB3 0WA, UK

This study considers the asymptotic Green's function and eigenmodes in a lined duct with swirling flow. We introduce the novel concept of the lining varying circumferentially, which then requires us to represent the impedance of the lining as a Fourier series and use the realistic limit of high frequency to calculate the eigenmodes and Green's function asymptotically. In previous work when the impedance is constant the high frequency limit has been shown to be a very good approximation to full numerical results, while for this case a full numerical solution is not currently possible.

Nomenclature

Latin Characters

A^j, B^j	Constants in solution v_j after using WKB method
$\boldsymbol{B^j} = (B_m^j)$	Finite vector of constants we solve for in asymptotic eigenmode problem when lining varies circumferentially
c_0	Base flow speed of sound
c_m, d_m	Fourier series coefficients of $1/Z(\theta)$
D_0/Dt	Base flow convective derivative
G	Green's function
G_n	Axial Fourier transform of the n-th azimuthal Fourier series coefficient of G_ω
G_ω	Reduced Green's function at a particular frequency in the duct
g_1, g_2	Solutions to the homogeneous equation that G_n solves with certain boundary conditions
h	Non-dimensionalised inner radius of the duct
i	Imaginary unit
J	Jump in first order derivative when finding the Green's function G_n
j	Used for indexing, $j \in \{1, 2\}$ or $j \in \{h, 1\}$
k	Axial wavenumber and eigenmode
k_n^m	A specific acoustic eigenmode indexed by m at a specific azimuthal number n
l	Used for indexing
M	Number of terms taken in truncated Fourier series of $1/Z(\theta)$
m	Used for indexing, generally $m \in \mathbb{Z}$ or $m \in \mathbb{N}$
n	Azimuthal number
$\underline{p}$	Total pressure of the flow
p	Pressure perturbation
p_0	Base flow pressure
q_n	Function in WKB differential equation. The number of zeros of q_n determines the form of the solution
r	Non-dimensionalised radial coordinate
r_n^c	Zero of q_n
$s^\pm$ $(s_n^\pm)$	Function used to find $\mathscr{K}$, $\mathscr{K} = s^+(\mathscr{R}) \cup s^-(\mathscr{R})$

*Research Associate, Department of Engineering, jrm214@cam.ac.uk. Professional member.

†Professor, Department of Applied Mathematics and Theoretical Physics, np100@cam.ac.uk. Senior member.

t	Time
$U_\theta(r)$	Swirl profile for base flow
$U_x(r)$	Shear profile for base flow
$(\underline{u}, \underline{v}, \underline{w})$	Total velocities of the flow (in x, r and θ directions respectively)
(u, v, w)	Velocity perturbations
(u_0, v_0, w_0)	Base flow velocities
v_1, v_2	Scaled versions of g_1 and g_2 used in WKB solution
x	Non-dimensionalised axial coordinate
$\boldsymbol{x} = (x, r, \theta)$	Cylindrical coordinates in the duct
$\boldsymbol{x_0} = (x_0, r_0, \theta_0)$	Source position in the duct
Z_j (Z)	Complex impedance of acoustic lining at duct walls
Z^a, Z^b, Z^c, Z^ς	Complex impedances of acoustic lining at duct walls which varies circumferentially
Greek Characters	
γ	Ratio of specific heat capacities
$\delta(f)$	Dirac delta
δ_{jl}	Kronecker delta
ϵ_r	Similar to Levi-Civita symbol, $\epsilon_h = 1$ and $\epsilon_1 = -1$
η	Scaled azimuthal number, $\eta = n/\omega$
θ	Circumferential coordinate
κ	Scaled axial wavenumber, $\kappa = k/\omega$
Λ^j	Finite matrix in asymptotic eigenmode problem when lining varies circumferentially
$\boldsymbol{\mu^j}$	Finite vector in asymptotic eigenmode problem when lining varies circumferentially
$\underline{\rho}$	Density of the total flow
ρ	Density perturbation
ρ_0	Base flow density
τ (τ_n)	Variables that the Airy functions act on in the WKB solution
$\Upsilon(\Upsilon_n)$	Function in differential equation for G_n
Υ_n^*	Scaled version of Υ_n, $\Upsilon_n = \omega\Upsilon_n^*$
Φ_n	Scaled version of Ω, $\Omega = \omega\Phi$
Ψ_n	Integral of $\sqrt{q_n}$ between r_c and 1, used in WKB method for one turning point solution
ψ_n	Integral of $\sqrt{q_n}$ in the duct, used in WKB method for zero turning point solution
Ω (Ω_n)	Function in differential equation for G_n, $\Omega = 0$ defines critical layer
ω	Non-dimensionalised frequency
Other Characters	
$\mathscr{A}_m$	Coefficient of constant A_m in $v_m(r)$
$\mathbb{A}_m$	Coefficient of constant A_m in $v_m'(r)$
$\mathscr{B}_m$	Coefficient of constant B_m in $v_m(r)$
$\mathbb{B}_m$	Coefficient of constant B_m in $v_m'(r)$
$\mathcal{F}$	Sixth order differential operator acting on pressure pertubation p in acoustic analogy
$\mathcal{K}_n^+$	Set of all acoustic downstream eigenmodes for a specific azimuthal number n
$\mathcal{K}_n^-$	Set of all acoustic upstream eigenmodes for a specific azimuthal number n
$\mathscr{K}$ $(\mathscr{K}_n)$	Region of κ space when we should use the one turning point solution in the WKB method
$\mathcal{R}$, $\mathcal{T}$	Differential operators in the acoustic analogy
$\mathscr{R}$	Region of r space when we should use the one turning point solution in the WKB method
$\mathcal{U}_\theta$	Function in differential equation for G_n which depends only on swirl U_θ
$\mathcal{V}$ $(\mathcal{V}_n)$	Wrońskian of v_1 and v_2
$\mathcal{W}$ $(\mathcal{W}_n)$	Wrońskian of g_1 and g_2
$\mathcal{X}_{n,m}$, $\mathcal{X}_{n,m}^*$	Coefficients in boundary condition for v_n when lining varies circumferentially
Other notation	
$\mathbb{1}_K$	Indicator function for a set K; $\mathbb{1}_K = \begin{cases} 1 & x \in K \\ 0 & x \in K^C \end{cases}$
Complement	The complement of a set K is $K^C = \mathbb{C}\backslash K$
Double dagger ‡	Quantities with dimension
Subscript $_0$	Base flow functions
Underlined	Total function, sum of perturbation and base flow

Abbreviations

WKB Wentzel-Kramers-Brillouin method[1] for solving a differential equation with a small parameter

I. Introduction

In this study we will calculate the Green's function and eigenmodes for swirling flow in a duct where the lining varies circumferentially. Previous work has considered the case of realistic swirling flow in a lined duct of fixed impedance (Mathews & Peake,[2] Posson & Peake[3]), or in swirling flow in a hard-walled duct (Posson & Peake[4]). We will derive an asymptotic dispersion relation for the eigenmodes in the high-frequency limit and then numerically solve it. We then use the work from Mathews & Peake[2] to calculate the asymptotic Green's function in swirling flow as the impedance of the acoustic lining varies circumferentially. The Green's function will be useful for calculating the pressure in rotor-stator interaction if we know the noise sources (as in Posson & Peake[4]), or it can be used in beamforming (see for example Sitjsma[5]) along with microphone measurements to calculate the noise sources.

By considering the impedance to be a discontinuous function, we can model splices in the lining. Splices are needed because the acoustic liner in the aeroengine duct is often made in two (or more) semicircular pieces and then joined together, and this join is not lined. Although both Airbus[a] and Rolls-Royce[b] have recently developed zero-splice liners, these are only applicable in the aeroengine inlet and not in the interstage between the rotor and stator. Thus, when studying rotor-stator interaction we need to consider the effect of splices. We can also consider lining when the impedance is a continuous function. For example, liners can be damaged during service, creating harder patches in the lining, so the impedance varies circumferentially. Or, we could deliberately choose the acoustic lining such that the impedance smoothly varies circumferentially to dampen some of the azimuthal modes. We will only consider the case of a smooth impedance function.

The eigenmode problem for splices has previously only been considered analytically for very simple cases of flow in the duct. The case of no flow was first considered by Fuller,[6] while Campos & Oliveira[7] extended this to uniform shear. However, their boundary condition was incorrect Brambley et al.[8] In Brambley et al.[8] the eigenmodes and Green's function were found for the case of uniform shear flow, exploiting the thinness of the splice to use asymptotic methods. It was shown that the splice only affected eigenmodes with small imaginary parts, while upstream modes are more affected than downstream modes.

A numerical method to calculate the eigenmodes in the spliced duct was given in Wright,[9] but only considers the case of no flow in the duct. Other numerical methods to consider the effect of splices include the multimodal method, which was developed in Pagneux et al.[10] and then considered in the case of no flow in Bi et al.[11] and uniform shear flow in Bi.[12] The effect of damaged splices was studied numerically by Mustafi et al.[13]

II. Examples of lining varying circumferentially

We allow the impedances of the acoustic lining at the duct walls to depend on the circumferential coordinate, so we consider $Z(\theta)$, and further assume the impedance is the same at both duct walls, although this is not necessary. We can choose the impedance function $Z(\theta)$ such that the impedance smoothly varies with θ or is discontinuous to model splices in the duct. Three important examples of impedance functions are given by

$$Z^a(\theta) = Z, \tag{1}$$

$$Z^b(\theta) = 1 - 2\mathrm{i}(\sin(2\theta) + 2), \tag{2}$$

$$\frac{1}{Z^c(\theta)} = \frac{1}{Z}\left[1 - \mathbb{1}_{-\frac{1}{2}<\theta<\frac{1}{2}}\right], \tag{3}$$

for Z of the form $Z = 1 - Z_{\mathrm{imag}}\mathrm{i}$, where Z_{imag} is positive. The first example is where the impedance is constant and we can use Mathews & Peake[2] to calculate the eigenmodes and Green's function. The second example is where the lining varies smoothly between $Z = 1 - 2\mathrm{i}$ and $Z = 1 - 6\mathrm{i}$. The third example is an

[a] http://www.technology-licensing.com/etl/int/en/What-we-offer/Technologies-for-licensing/Green-Technologies/Zero-splice-air-inlet-for-jet-engines.html

[b] http://www.rolls-royce.com/sustainability/performance/case-studies/noise-technology.aspx

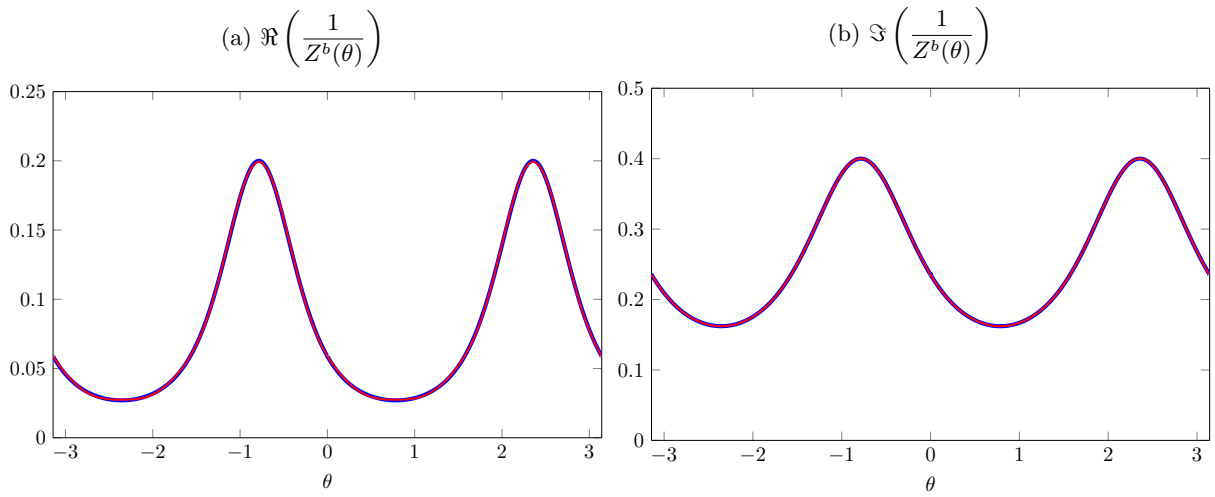

Figure 1: Real and imaginary part of the truncated Fourier series of $1/Z^b(\theta)$ when $M = 8$ (red) and $1/Z^b(\theta)$ (blue).

example of when we consider a single splice in the duct for $-\frac{1}{2} < \theta < \frac{1}{2}$. The splice is used to join together pieces of acoustic lining, and the splice has hard walls with $Z^c(\theta) = \infty$. Away from the splice $Z^c(\theta) = Z$.

Often, there is more than one splice and the splices would be relatively thin. We could exploit the thinness of the splicing as a small parameter and perform asymptotics similar to Brambley.[8] Instead, we use the high-frequency asymptotic method from Mathews & Peake,[2] but with different boundary conditions, which allows us to consider arbitrary forms of $Z(\theta)$.

It will be necessary to represent the impedance function as a Fourier series, in the form

$$\frac{1}{Z(\theta)} = \sum_{m=-\infty}^{\infty} d_m e^{\mathrm{i}m\theta} \text{ or } \frac{1}{Z(\theta)} = \sum_{m=-\infty}^{\infty} c_m(\theta_0) e^{\mathrm{i}m(\theta-\theta_0)}. \tag{4}$$

For some sufficiently large M, we can truncate the series, with

$$\frac{1}{Z(\theta)} \approx \sum_{m=-M}^{M} d_m e^{\mathrm{i}m\theta} \text{ or } \frac{1}{Z(\theta)} \approx \sum_{m=-M}^{M} c_m(\theta_0) e^{\mathrm{i}m(\theta-\theta_0)} \tag{5}$$

The Fourier series of $Z^a(\theta)$ only has one non-zero term. In Figure 1 we plot the truncated Fourier series for $1/Z^b(\theta)$ in red when $M = 8$. We plot the function $1/Z^b(\theta)$ in blue and we see the approximation is very good, with an error of $\mathcal{O}(10^{-4})$. The reason we could take so few terms in the truncated Fourier series is the smoothness of $Z^b(\theta)$. By contrast, we need to take a significant number of terms in the truncated Fourier series for $Z^c(\theta)$. In Figure 2 we plot the truncated Fourier series for $M = 10$, $M = 30$ and $M = 100$. We see that we need a significant amount of terms in the truncation to accurately approximate the original impedance function, and furthermore Gibbs phenomena occurs near $\theta = \pm 1/2$.

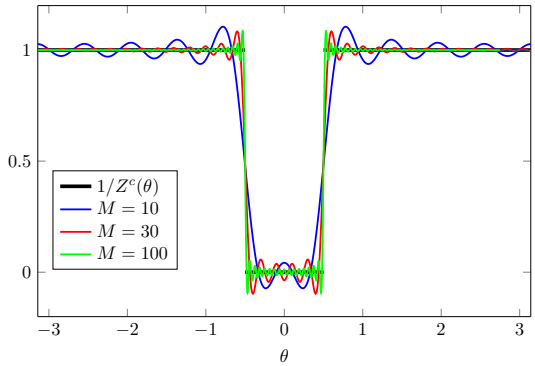

Figure 2: Plot of truncated Fourier series of $1/Z^c(\theta)$ (black) for $M = 10$ (blue), $M = 30$ (red), $M = 100$ (green).

III. Swirling base flow

We will model the aeroengine as an infinite cylindrical duct. Let the inner and outer duct walls be given by $r^\ddagger = h^\ddagger$ and $r^\ddagger = d^\ddagger$ respectively, where the double dagger $\ddagger$ represents dimensioned coordinates. We non-dimensionalise all distances by $d^\ddagger$, so that the inner wall lies at $r = h := h^\ddagger/d^\ddagger$ and the outer wall at $r = 1$. We non-dimensionalise all velocities by the speed of sound at $r = 1$, $c_0^\ddagger(d^\ddagger)$. Finally, we non-dimensionalise time by $d^\ddagger/c_0^\ddagger(d^\ddagger)$ and all frequencies by $c_0^\ddagger(d^\ddagger)/d^\ddagger$. The impedance is non-dimensionalised such that $Z = Z^\ddagger/(\rho_0^\ddagger(d^\ddagger)c_0^\ddagger(d^\ddagger))$.

We use a standard cylindrical coordinate system, with x the axial coordinate, r the radial coordinate and θ the azimuthal coordinate. We let $\underline{u}$, $\underline{v}$ and $\underline{w}$ be the velocities in the x, r and θ directions respectively. We split the inviscid total flow (underlined) into a base flow (subscript 0) plus some small perturbations, so we have

$$(\underline{u}, \underline{v}, \underline{w}, \underline{\rho}, \underline{p}) = (u_0, v_0, w_0, \rho_0, p_0) + (u, v, w, \rho, p), \tag{6}$$

where $\underline{\boldsymbol{u}} = (\underline{u}, \underline{v}, \underline{w})$ is the total velocity of the air, $\underline{\rho}$ is the total density and $\underline{p}$ the total pressure.

The swirling base flow is a solution of the Euler equations, which we define by specifying the base flow velocities, and then calculate the pressure, density and speed of sound. We assume a homentropic flow so the entropy is constant, and that the fluid is a perfect gas. We choose a base flow of the form

$$(u_0, v_0, w_0) = (U_x(r), 0, U_\theta(r)), \tag{7}$$

where $U_x(r)$ and $U_\theta(r)$ are freely chosen. This will give a base flow representative of swirling mean flow (see Mathews & Peake[2]). The speed of sound c_0 is given by

$$c_0^2(r) = c_0^2(1) + (\gamma - 1)\int_1^r \frac{U_\theta^2(s)}{s}\mathrm{d}s, \tag{8}$$

where γ is the ratio of specific heat capacities ($\gamma = 1.4$ for air). The density and pressure are then given by

$$\rho_0(r) = [c_0^2(r)]^{1/(\gamma-1)} \text{ and } p_0(r) = p_0(1) - \int_r^1 \frac{\rho_0(s)U_\theta^2(s)}{s}\mathrm{d}s. \tag{9}$$

IV. Green's function with new boundary conditions

In this section we find the Green's function $G_\omega(\boldsymbol{x}|\boldsymbol{x}_0)$ of the sixth order differential operator $\mathcal{F}$, which is defined in both Mathews & Peake[2] and Posson & Peake,[4] but now with the impedance of the acoustic lining varying circumferentially. The differential equation for the Green's function remains unchanged, while the boundary conditions become significantly more complicated and coupled.

A. Green's function

The Green's function $G_\omega(\boldsymbol{x}|\boldsymbol{x}_0)$ satisfies

$$\mathcal{F}\left(G_\omega(\boldsymbol{x}|\boldsymbol{x}_0)e^{-\mathrm{i}\omega t}\right) = \delta(\boldsymbol{x} - \boldsymbol{x}_0)e^{-\mathrm{i}\omega t} = \delta(x - x_0)\frac{\delta(r - r_0)}{r}\delta(\theta - \theta_0)e^{-\mathrm{i}\omega t}, \tag{10}$$

and we look for a Green's function of the form

$$G_\omega(\boldsymbol{x}|\boldsymbol{x}_0) = \frac{1}{4\pi^2}\sum_{n=-\infty}^{\infty} e^{\mathrm{i}n(\theta-\theta_0)}\int_{\mathbb{R}} G_n(r|r_0;\omega,k)e^{\mathrm{i}k(x-x_0)}\mathrm{d}k. \tag{11}$$

We find it is given by (using Bender & Orszag[1])

$$G_n(r|r_0;\omega,k,n) = \frac{1}{r_0\mathcal{W}_n(r_0)J_n(r_0,k)}\begin{cases} g_n^1(r_0;\omega,k)g_n^2(r;\omega,k) & r \le r_0 \\ g_n^2(r_0;\omega,k)g_n^1(r;\omega,k) & r > r_0 \end{cases}, \tag{12}$$

where $J_n(r_0,k) = \left[\Omega^2(r_0,k) - \mathcal{U}_\theta(r_0)\right]\Omega^2(r_0,k)$ and the Wrońskian is given by

$$\mathcal{W}_n(r_0;\omega,k,n) = g_n^1(r_0;\omega,k)\frac{\mathrm{d}g_n^2}{\mathrm{d}r}(r_0;\omega,k) - \frac{\mathrm{d}g_n^1}{\mathrm{d}r}(r_0;\omega,k)g_n^2(r_0;\omega,k). \tag{13}$$

The functions g_n^j satisfy

$$\frac{p_0}{c_0^2 r}(\mathcal{U}_\theta - \Omega^2)^2\Omega^2 \frac{\mathrm{d}}{\mathrm{d}r}\left(\frac{rc_0^2}{p_0(\Omega^2 - \mathcal{U}_\theta)}\frac{\mathrm{d}g_n^j}{\mathrm{d}r}\right) + \left[(\mathcal{U}_\theta - \Omega^2)^2\left(\frac{\Omega^2}{c_0^2} - k^2 - \frac{n^2}{r^2}\right)\right. \tag{14}$$
$$\left. + \Upsilon(\mathcal{U}_\theta - \Omega^2)\left[\Upsilon + \Omega\left(\frac{1}{r} - \frac{\rho_0'}{\rho_0}\right)\right] - \Upsilon'\Omega(\Omega^2 - \mathcal{U}_\theta) + \Upsilon[\Omega(\Omega^2 - \mathcal{U}_\theta)]'\right] g_n^j = 0,$$

where the functions Ω, Υ and $\mathcal{U}_\theta$ are defined as

$$\mathcal{U}_\theta(r) = \frac{2U_\theta(r)}{r^2}\frac{\mathrm{d}}{\mathrm{d}r}(rU_\theta) + \frac{U_\theta^2(r)}{r}\left(\frac{\rho_0'(r)}{\rho_0(r)} - \frac{U_\theta^2(r)}{rc_0^2(r)}\right), \tag{15}$$

and

$$\Omega(r) = \omega - kU_x(r) - \frac{nU_\theta(r)}{r} \text{ and } \Upsilon(r) = \frac{U_\theta^2(r)}{rc_0^2(r)}\Omega(r) + \frac{2nU_\theta(r)}{r^2}., \tag{16}$$

B. Boundary conditions

We write the standard Myers or Ingard-Myers[14,15] boundary condition as

$$\mathrm{i}\omega v = \frac{D_0}{Dt}\left(\frac{p}{Z(\theta)}\right) \text{ on } r = h \text{ and } -\mathrm{i}\omega v = \frac{D_0}{Dt}\left(\frac{p}{Z(\theta)}\right) \text{ on } r = 1, \tag{17}$$

where we assume the time dependence of $p \propto e^{-\mathrm{i}\omega t}$. It was shown in Masson et al.[16] that the Myers boundary condition was not the correct limit of an infinitely thin boundary layer in swirling flow, and instead we should replace $Z(\theta)$ by $Z(\theta)$ plus a centrifugal term if we are modelling a swirling flow with an infinitely thin boundary layer. However, the analysis follows in the same way as, so for consistency will previous results we will use the classical Myers boundary condition. We then apply the operator $\mathcal{R}$ from before to both sides and use $\rho_0\mathcal{R}(v) = \mathcal{T}(p)$ (which holds when there are no source terms), where

$$\mathcal{R} = \frac{{D_0}^2}{Dt^2} + \mathcal{U}_\theta \text{ and } \mathcal{T} = -\frac{D_0}{Dt}\frac{\partial}{\partial r} - \frac{2U_\theta}{r^2}\frac{\partial}{\partial\theta} + \frac{U_\theta^2}{rc_0^2}\frac{D_0}{Dt}. \tag{18}$$

After some rearrangement, we find that

$$\epsilon_r\frac{\mathrm{i}\omega\mathcal{T}(p)}{\rho_0} = \frac{1}{Z(\theta)}\mathcal{R}\left(\frac{D_0 p}{Dt}\right) + \left(\frac{1}{Z(\theta)}\right)'\left[\frac{2U_\theta}{r}\frac{D_0^2 p}{Dt^2} + \frac{U_\theta}{r}\mathcal{R}(p)\right] + \left(\frac{1}{Z(\theta)}\right)''\frac{3U_\theta^2}{r^2}\frac{D_0 p}{Dt} + \left(\frac{1}{Z(\theta)}\right)'''\frac{U_\theta^3}{r^3}p \tag{19}$$

for $r = h$, 1 where $\epsilon_h = 1$ and $\epsilon_1 = -1$. Setting $Z(\theta) = Z$, a constant, reduces the boundary conditions to

$$\epsilon_r\frac{\mathrm{i}\omega\mathcal{T}(p)}{\rho_0} = \frac{1}{Z}\frac{D_0}{Dt}\mathcal{R}(p), \tag{20}$$

since $\mathcal{R}$ and the material derivative always commute. Thus, we recover the boundary conditions from Mathews[2] for a constant impedance. We would also get a boundary condition of the form in (20) when there is no swirl but the lining varies circumferentially.

We now substitute in $G_\omega(\boldsymbol{x}|\boldsymbol{x}_0)e^{-\mathrm{i}\omega t}$ to (19), using the form of G_ω in (11). Next, we write the impedance as a truncated Fourier series with coefficients $c_m(\theta_0)$, which differ by a factor of $e^{\mathrm{i}m\theta_0}$ compared to the standard Fourier series coefficients d_m as seen in (5). We easily calculate the Fourier series of the l-th derivative of $1/Z$, with the Fourier coefficients given by $(\mathrm{i}m)^l c_m(\theta_0)$. Substituting the truncated Fourier

series into (19), and then using the convolution theorem gives

$$
\begin{aligned}
-\epsilon_r \frac{\omega}{\rho_0}\left[\Omega_n \frac{\mathrm{d}G_n}{\mathrm{d}r} - \Upsilon_n G_n\right] = & \sum_{m=n-M}^{n+M} c_{n-m}(\theta_0)(-\mathrm{i}\Omega_m)(\mathcal{U}_\theta - \Omega_m^2) G_m \\
& + \sum_{m=n-M}^{n+M} \mathrm{i}(n-m) c_{n-m}(\theta_0)\left[\frac{U_\theta}{r}(\mathcal{U}_\theta - \Omega_m^2) - \Omega_m^2 \frac{2U_\theta}{r}\right] G_m \\
& + \sum_{m=n-M}^{n+M} (n-m)^2 c_{n-m}(\theta_0) 3\mathrm{i}\Omega_m \frac{U_\theta^2}{r^2} G_m \\
& - \sum_{m=n-M}^{n+M} \mathrm{i}(n-m)^3 c_{n-m}(\theta_0) \frac{U_\theta^3}{r^3} G_m,
\end{aligned} \tag{21}
$$

for $r = h$ and $r = 1$. To find the Green's function we thus solve (14) for $g_n^1(r;\omega,k)$ and $g_n^2(r;\omega,k)$, where $g_n^1(r;\omega,k)$ solves the boundary condition (21) for $r = 1$ and $g_n^2(r;\omega,k)$ solves the boundary condition (21) for $r = h$. We then use (12) to calculate G_n. We will have to solve a coupled system of equations to determine $g_n^j(r;\omega,k)$, unless the impedance is constant.

When there is no swirl, the boundary conditions simplify significantly and we solve

$$
-\epsilon_r \frac{\omega}{\rho_0}\Omega_n \frac{\mathrm{d}G_n}{\mathrm{d}r} = \sum_{m=n-M}^{n+M} c_{n-m}(\theta_0)\mathrm{i}\Omega_m^3 G_m, \tag{22}
$$

although we still have a coupled system.

V. High frequency asymptotic solution

We now consider the high-frequency limit, so we assume that the frequency $k = \mathcal{O}(\omega)$, where ω is large, so that $k = \kappa\omega$ with $\kappa = \mathcal{O}(1)$. We also assume that $n = \mathcal{O}(\omega)$.

A. Differential equation in high-frequency limit

The differential equation that $g_n^j(r;\kappa)$ satisfies in the high-frequency limit is given by (see Mathews[17])

$$
\frac{\mathrm{d}^2 g_n^j}{\mathrm{d}r^2}(r;\kappa) + \left(\frac{1}{r} - \frac{\rho_0'(r)}{\rho_0(r)} - 2\frac{\frac{\partial}{\partial r}\Phi_n(r,\kappa)}{\Phi_n(r,\kappa)}\right)\frac{\mathrm{d}g_n^j}{\mathrm{d}r}(r;\kappa) + \omega^2 q_n(r,\kappa) g_n^j(r;\kappa) = 0, \tag{23}
$$

where

$$
\Phi_n(r,\kappa) = 1 - \kappa U_x(r) - \frac{nU_\theta}{\omega r} \text{ and } q_n(r,\kappa) := \left(\frac{\Phi_n^2(r,\kappa)}{c_0^2(r)} - \kappa^2 - \frac{n^2}{\omega^2 r^2}\right), \tag{24}
$$

with $\omega\Phi_n = \Omega$. We introduce the change of variables

$$
g_n^j(r;\kappa) = \frac{\rho_0^{1/2}(r)\Phi_n(r,\kappa) v_n^j(r;\kappa)}{r^{1/2}}, \tag{25}
$$

and then we look for solutions to the equation

$$
\frac{\mathrm{d}^2 v_n^j}{\mathrm{d}r^2}(r;\kappa) + \left[\omega^2 q_n(r,\kappa) + q_n^*(r,\kappa)\right] v_n^j(r;\kappa) = 0, \tag{26}
$$

where q_n^* is irrelevant for the leading order solution. The Green's function is then given by

$$
G_n(r|r_0;\kappa) = \left(\frac{\rho_0(r) r_0}{\rho_0(r_0) r}\right)^{1/2} \frac{\Phi_n(r,\kappa)}{r_0 \mathcal{V}_n(r_0,\kappa) J_n(r_0,\kappa)\Phi_n(r_0,\kappa)} \begin{cases} v_n^1(r_0;\kappa) v_n^2(r;\kappa) & r \le r_0 \\ v_n^2(r_0;\kappa) v_n^1(r;\kappa) & r > r_0 \end{cases}, \tag{27}
$$

where the Wrońskian

$$
\mathcal{V}_n(r_0,\kappa) = v_n^1(r_0;\kappa)\frac{\mathrm{d}v_n^2}{\mathrm{d}r}(r_0;\kappa) - \frac{\mathrm{d}v_n^1}{\mathrm{d}r}(r_0;\kappa) v_n^2(r_0;\kappa), \tag{28}
$$

is now independent of r_0 by Abel's theorem (Boyce et al[18]). When κ is an eigenmode then $\mathcal{V}_n$ is identically zero.

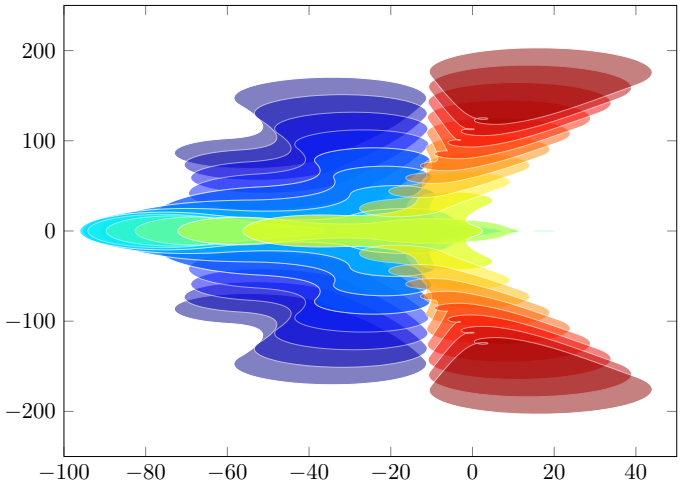

Figure 3: Plot of regions $\omega\mathscr{K}_n$ as n varies from $n=-100$ (blue) to $n=100$ (red). We only plot intervals of $n=10$. The other parameters of the flow are $\omega=25$, $h=0.6$, $U_x(r)=0.2+0.4r^2$ and $U_\theta(r)=0.1r+0.2/r$.

B. High frequency WKB solution

We solve the differential equation in (26) using the WKB method, as in Mathews & Peake.[2] The solution depends on how many zeros $q_n(r,\kappa)$ has near the duct, and we only consider the case when there is at most one zero for convenience. In Mathews & Peake[2] the case when $q_n(r,\kappa)$ has two or more zeros is considered, although this requires more numerics. We find there are two different possible forms for the solutions, when $\kappa\in\mathscr{K}_n$ and when $\kappa\in\mathscr{K}_n^C$. For $\kappa\in\mathscr{K}_n$, $q_n(r,\kappa)$ has a single zero near the duct and the WKB solution is a linear combination of Airy functions. For $\kappa\in\mathscr{K}_n^C$, $q_n(r,\kappa)$ has no zeros near the duct and hence the solution is given by a linear combination of exponentials or sines and cosines.

We define the region of κ space where we use the Airy solution, $\mathscr{K}_n$, as in Mathews & Peake,[2] so $\mathscr{K}_n=s_n^+(\mathscr{R})\cup s_n^-(\mathscr{R})$ where $\mathscr{R}=\left\{r\in\mathbb{C}\,\middle|\,|r-r_1|<\omega^{-2/3}\text{ for }r_1\in[h,1]\right\}$ and

$$s_n^\pm(r)=\frac{U_x(r)\left(1-\frac{nU_\theta(r)}{\omega r}\right)\pm c_0(r)\sqrt{\left(1-\frac{nU_\theta(r)}{\omega r}\right)^2+\frac{n^2}{\omega^2r^2}[U_x^2(r)-c_0^2(r)]}}{U_x^2(r)-c_0^2(r)}. \tag{29}$$

In Figure 3 we plot how $\omega\mathscr{K}_n$ changes as we vary n for a typical swirling flow.

We find that the WKB solution is given by

$$v_n^j(r;\kappa)=A_n^j(\kappa)\mathscr{A}_n(r;\kappa)+B_n^j(\kappa)\mathscr{B}_n(r;\kappa), \tag{30}$$

where

$$\mathscr{A}_n(r;\kappa)=\frac{1}{1+\mathrm{i}}|q_n(r,\kappa)|^{-1/4}e^{\mathrm{i}\omega\psi_n(r,\kappa)}\mathbb{1}_{\mathscr{K}_n^C}+\sqrt{\pi}\left[\left(\frac{\tau_n(r,\kappa)}{q_n(r,\kappa)}\right)^{1/4}\mathrm{Ai}\left(-\tau_n(r,\kappa)\right)\right]\mathbb{1}_{\mathscr{K}_n}, \tag{31}$$

and

$$\mathscr{B}_n(r;\kappa)=\frac{1}{1+\mathrm{i}}|q_n(r,\kappa)|^{-1/4}e^{-\mathrm{i}\omega\psi_n(r,\kappa)}\mathbb{1}_{\mathscr{K}_n^C}+\sqrt{\pi}\left[\left(\frac{\tau_n(r,\kappa)}{q_n(r,\kappa)}\right)^{1/4}\mathrm{Bi}\left(-\tau_n(r,\kappa)\right)\right]\mathbb{1}_{\mathscr{K}_n}, \tag{32}$$

with

$$\tau_n(r,\kappa)=\left(\frac{3\omega\Psi_n(r,\kappa)}{2}\right)^{2/3}, \tag{33}$$

and $\mathbb{1}$ the indicator function. The functions $\psi_n(r,\kappa)$ and $\Psi_n(r,\kappa)$ are defined by

$$\psi_n(r,\kappa)=\int_h^1\sqrt{q_n(s,\kappa)}\mathrm{d}s\text{ and }\Psi_n(r,\kappa)=\int_{r_n^c(\kappa)}^1\sqrt{q_n(s,\kappa)}\mathrm{d}s, \tag{34}$$

where $r_n^c(\kappa)$ is such that $q_n(r_n^c(\kappa),\kappa)=0$. To determine $A_n^j(\kappa)$ and $B_n^j(\kappa)$ we use the coupled boundary conditions. When considering the branch cuts of the non-integer roots, we found that as long as we didn't cross the branch cut, any choice was acceptable.

When applying the boundary conditions, it will be necessary to find the radial derivatives of $v_n^j(r,\kappa)$, which can be found in Mathews,[17] of the form

$$\frac{\mathrm{d}v_n^j}{\mathrm{d}r}(r;\kappa)=A_n^j(\kappa)\mathbb{A}_n(r,\kappa)+B_n^j(\kappa)\mathbb{B}_n(r,\kappa), \tag{35}$$

where

$$\mathbb{A}_n(r,\kappa)=\frac{1}{1+\mathrm{i}}\left(-\frac{\frac{\partial}{\partial r}q_n(r,\kappa)}{4q_n(r,\kappa)}+\mathrm{i}\omega\sqrt{q_n(r,\kappa)}\right)|q_n(r,\kappa)|^{-1/4}e^{\mathrm{i}\omega\psi_n(r,\kappa)}\mathbb{1}_{\mathscr{K}_n^C}+\sqrt{\pi}\left(\frac{\tau_n(r,\kappa)}{q_n(r,\kappa)}\right)^{1/4}\times$$
$$\left[\left(\frac{1}{6}\frac{\frac{\partial}{\partial r}\Psi_n(r,\kappa)}{\Psi_n(r,\kappa)}-\frac{1}{4}\frac{\frac{\partial}{\partial r}q_n(r,\kappa)}{q_n(r,\kappa)}\right)\mathrm{Ai}(-\tau_n(r,\kappa))-\frac{2}{3}\frac{\frac{\partial}{\partial r}\Psi_n(r,\kappa)}{\Psi_n(r,\kappa)}\tau_n(r,\kappa)\,\mathrm{Ai}'(-(\tau_n(r,\kappa))\right]\mathbb{1}_{\mathscr{K}_n}, \tag{36}$$

and

$$\mathbb{B}_n(r,\kappa)=\frac{1}{1+\mathrm{i}}\left(-\frac{\frac{\partial}{\partial r}q_n(r,\kappa)}{4q_n(r,\kappa)}-\mathrm{i}\omega\sqrt{q_n(r,\kappa)}\right)|q_n(r,\kappa)|^{-1/4}e^{-\mathrm{i}\omega\psi_n(r,\kappa)}\mathbb{1}_{\mathscr{K}_n^C}+\sqrt{\pi}\left(\frac{\tau_n(r,\kappa)}{q_n(r,\kappa)}\right)^{1/4}\times$$
$$\left[\left(\frac{1}{6}\frac{\frac{\partial}{\partial r}\Psi_n(r,\kappa)}{\Psi_n(r,\kappa)}-\frac{1}{4}\frac{\frac{\partial}{\partial r}q_n(r,\kappa)}{q_n(r,\kappa)}\right)\mathrm{Bi}(-\tau_n(r,\kappa))-\frac{2}{3}\frac{\frac{\partial}{\partial r}\Psi_n(r,\kappa)}{\Psi_n(r,\kappa)}\tau_n(r,\kappa)\,\mathrm{Bi}'(-(\tau_n(r,\kappa))\right]\mathbb{1}_{\mathscr{K}_n}, \tag{37}$$

C. High frequency boundary conditions

After inserting $v_n^j(r,\kappa)$ into the boundary conditions in (21), via the change of variables in (25), we find that

$$-\frac{\omega}{\rho_0(h)}\Phi_n^2(h,\kappa)\frac{\mathrm{d}v_n^2}{\mathrm{d}r}(h;\kappa)=\sum_{m=n-M}^{n+M}\left[c_{n-m}(\theta_0)\mathcal{X}_{n,m}(h,\kappa)+\mathcal{X}_{n,m}^*(h,\kappa)\right]v_m^2(h;\kappa), \tag{38}$$

and

$$\frac{\omega}{\rho_0(1)}\Phi_n^2(1,\kappa)\frac{\mathrm{d}v_n^1}{\mathrm{d}r}(1;\kappa)=\sum_{m=n-M}^{n+M}\left[c_{n-m}(\theta_0)\mathcal{X}_{n,m}(1,\kappa)+\mathcal{X}_{n,m}^*(1,\kappa)\right]v_m^1(1;\kappa), \tag{39}$$

where

$$\mathcal{X}_{n,m}(r,\kappa)=\Phi_m(r,\kappa)\left(\mathrm{i}\omega^2\left(\Phi_m(r,\kappa)-\frac{n-m}{\omega}\frac{U_\theta(r)}{r}\right)^3-\mathrm{i}\left[\frac{n-m}{\omega}\frac{U_\theta(r)\mathcal{U}_\theta(r)}{r}-\Phi_m(r,\kappa)\mathcal{U}_\theta(r)\right]\right), \tag{40}$$

and

$$\mathcal{X}_{n,m}^*(r,\kappa)=\delta_{mn}\epsilon_r\frac{\omega}{\rho_0(r)}\left[-\Upsilon_m^*(r,\kappa)\Phi_m(r,\kappa)+\frac{\Phi_m^2(r,\kappa)}{2}\left(\frac{\rho_0'(r)}{\rho_0(r)}-\frac{1}{r}+2\frac{\frac{\partial}{\partial r}\Phi_m(r,\kappa)}{\Phi_m(r,\kappa)}\right)\right], \tag{41}$$

with δ_{mn} the Kronecker delta and $\Upsilon=\omega\Upsilon^*$. In the high-frequency limit we could ignore the $\mathcal{X}_{n,m}^*$ term and use the approximation

$$\mathcal{X}_{n,m}(r,\kappa)\approx\mathrm{i}\omega^2\Phi_m(r,\kappa)\left(\Phi_m(r,\kappa)-\frac{n-m}{\omega}\frac{U_\theta(r)}{r}\right)^3, \tag{42}$$

but we will use the full form of $\mathcal{X}_{n,m}$ and $\mathcal{X}_{n,m}^*$.

D. Calculating the Wrońskian and eigenmodes asymptotically

We now set $A_n^1 = A_n^h = 1$, and then calculated the Wrońskian $\mathcal{V}_n(\kappa)$. After using the properties of the Airy function we find that dispersion relation is given by

$$\mathcal{V}_n(\kappa) = \omega \left[B_n^1(\kappa) - B_n^h(\kappa) \right]. \tag{43}$$

It remains to calculate B_n^1 and B_n^h. To do this we substitute the WKB solution into the boundary conditions in (38) and (39). This then gives a infinite matrix value problem to solve to find B_n^1 and B_n^h. We truncate this to a finite matrix problem by setting $G_n = 0$ for $|n| > N$, where we need to choose N sufficiently large. We then get a problem of the form

$$\Lambda^j \boldsymbol{B^j} = \boldsymbol{\mu^j}, \tag{44}$$

where

$$\boldsymbol{B^j} = [B_{-N}^j, \ldots, B_{-1}^j, B_0^j, B_1^j, \ldots, B_N^j]^T. \tag{45}$$

If we let $N_1 = 2N + 1$, then $\boldsymbol{\mu^j}$ is a column vector of size N_1, while Λ^j is a square matrix of size $N_1 \times N_1$, and is of the form

$$\Lambda^j = \begin{bmatrix}
\times & \times & \times & 0 & & & & & \\
\times & \times & \times & \times & 0 & & & & \\
\times & \times & \times & \times & \times & 0 & & & \\
0 & \times & \times & \times & \times & \times & 0 & & \\
 & 0 & \times & \times & \times & \times & \times & 0 & \\
 & & 0 & \ddots & \ddots & \ddots & \ddots & \ddots & 0 \\
 & & & 0 & \times & \times & \times & \times & \times \\
 & & & & 0 & \times & \times & \times & \times \\
 & & 0 & & & 0 & \times & \times & \times \\
 & & & & & & 0 & \times & \times
\end{bmatrix}, \tag{46}$$

when $M = 2$, with $\times$ symbols representing non-zero entries. If we index the diagonals of Λ^h by l, with $l = 0$ corresponding to the main (or principle) diagonal, then for $|l| \leq M$ we have

$$\mathrm{diag}(\Lambda^j, l) = (\Lambda_{n,l}^j(\kappa))_{n=\max(-N,-N-l)}^{n=\min(N,N-l)}, \tag{47}$$

where

$$\Lambda_{n,l}^j(\kappa) = -\left[c_{-l}(\theta_0) \mathcal{X}_{n,n+l}(r_j, \kappa) + \mathcal{X}_{n,n+l}^*(r_j, \kappa) \right] \mathscr{B}_{n+l}^j(\kappa) - \epsilon_{r_j} \delta_{l0} \frac{\omega}{\rho_0(r_j)} \Phi_{n+l}^2(r_j, \kappa) \mathbb{B}_{n+l}^j(\kappa), \tag{48}$$

with $r_1 = 1$ and $r_2 = h$. For $|l| > M$ the diagonal is exactly zero. The vector $\boldsymbol{\mu_j}$ is given by

$$\boldsymbol{\mu}^j = \left(\mu_n^j(\kappa) \right)_{n=-N}^{n=N}, \tag{49}$$

where

$$\mu_n^j(\kappa) = \sum_{m=\max(n-M,-N)}^{\min(n+M,N)} \left[c_{n-m}(\theta_0) \mathcal{X}_{n,m}(r_j, \kappa) + \mathcal{X}_{n,m}^*(r_j, \kappa) \right] \mathscr{A}_m^j(\kappa) + \epsilon_{r_j} \frac{\omega}{\rho_0(r_j)} \Phi_n^2(r_j, \kappa) \mathbb{A}_n^j(\kappa). \tag{50}$$

E. Calculating the Green's function asymptotically

We now discuss how to find the Green's function when the lining varies circumferentially. We only consider the contribution from the acoustic modes, since from Posson & Peake[4] we expect the the contribution from the critical layer to be generally very small but very expensive to calculate.

The total contribution from the acoustic eigenmodes is given by

$$G_\omega^A(\boldsymbol{x}|\boldsymbol{x}_0) = \sum_{n=-\infty}^{\infty} e^{\mathrm{i}n(\theta-\theta_0)} \sum_{\mathcal{K}_n^\pm} \widehat{G}_n^m(x, r|x_0, r_0), \tag{51}$$

where

$$\widehat{G}_n^m(x,r|x_0,r_0) = \pm\frac{2\pi\mathrm{i}\omega}{4\pi^2}\left(\frac{\rho_0(r)r_0}{\rho_0(r_0)r}\right)^{1/2}\frac{\Phi_n(r,\kappa_n^m)e^{\mathrm{i}\omega\kappa_n^m(x-x_0)}}{r_0 J_n(r_0,\kappa)\frac{\partial\mathcal{V}_n}{\partial\kappa}(\kappa_n^m)\Phi_n(r_0,\kappa_n^m)}\begin{cases} v_n^1(r_0;\kappa_n^m)v_n^2(r;\kappa_n^m) & r\le r_0 \\ v_n^2(r_0;\kappa_n^m)v_n^1(r;\kappa_n^m) & r>r_0 \end{cases}, \tag{52}$$

with the $\pm$ from $x-x_0>0$ or $x-x_0<0$. The set $\mathcal{K}_n^+$ consists of all downstream acoustic modes and $\mathcal{K}_n^-$ consists of all the upstream acoustic modes.

It remains to calculate the derivative of the Wrońskian, since we have already found v_n^1 and v_n^2. This is given by

$$\frac{\partial\mathcal{V}_n}{\partial\kappa}(\kappa_n^m) = \omega\left[\frac{\partial B_n^1}{\partial\kappa}(\kappa_n^m) - \frac{\partial B_n^h}{\partial\kappa}(\kappa_n^m)\right]. \tag{53}$$

The derivatives of B_n^j can either be calculated analytically (by differentiating (44) with respect to κ) or numerically.

VI. Results

We only consider results when the impedance of the lining is smooth, and we choose an impedance function of the form

$$Z^\varsigma(\theta) = 1 - 2\mathrm{i}\left(\varsigma\sin(2\theta)+2\right), \tag{54}$$

for different values of ς. When $\varsigma=0$ this corresponds to a constant impedance of $Z=1-4\mathrm{i}$. When $\varsigma=1$ this corresponds to an impedance oscillating between $Z=1-2\mathrm{i}$ and $Z=1-6\mathrm{i}$. We see the different values of ς we choose in Figure 4b.

The reason for not considering splices is that if we take sufficiently many terms in the Fourier series of the impedance to be accurate (large M), then we get large, badly conditioned matrices $\boldsymbol{B}^j$. When we then solve $\Lambda^1\boldsymbol{B}^{\boldsymbol{1}}=\boldsymbol{\mu}^{\boldsymbol{1}}$, we are unable to get a solution because of the badly conditioned matrix $\boldsymbol{B}^{\boldsymbol{1}}$.

We consider the swirling flow $U_x(r)=0.2+0.4r^2$ and $U_\theta(r)=0.1r+0.2/r$, which is a representative example to try. We additionally set $h=0.6$, $\omega=25$ and $\theta_0=0$. The regions $\mathscr{K}_n$ were plotted in Figure 3.

In Figure 4 we plot both the cut-on and cut-off eigenmodes. We find all the asymptotic modes for each impedance function, with the eigenmodes plotted in different colours depending on the impedance, with the legend in Figure 4b. We find that the asymptotic eigenmodes when $Z=1-4\mathrm{i}$ (blue circles) are very accurate compared to the numerical eigenmodes (black crosses), except at the first upstream and downstream cut-off mode, which is because they are close to the edge of the one turning point region, but we have used the exponential WKB solution.

For most of the upstream cut-off modes in Figure 4a we find as the impedance of the lining varies more (increasing ς), then the cut-off modes shift right, while the downstream cut-off modes mostly shift left. However, some cut-off modes with a large imaginary part shift in the opposite direction, as does the first downstream cut-off mode.

For the cut-on eigenmodes, it is clear that the modes do not move by that much in Figure 4e, and we see a close up of their trajectories in Figure 5. In Figure 5 we also plot in grey extra eigenmodes, which are for impedances Z^ς where ς takes the midpoint of the two values of ς of the coloured eigenmodes. For the upstream modes, as we increase ς then the modes generally shift left and down in the complex plane, although the first and second upstream modes initially move upwards. For the downstream modes, the second and third downstream modes move right and initially down and then upwards. The first downstream mode has more peculiar behaviour, firstly moving right and down and then moving left and up. From Figure 5 we see that the upstream eigenmodes move more than the downstream eigenmodes, which is in agreement with the results from Brambley et al.[8]

Next, we consider the Green's function for each eigenmode as we vary the impedance function Z^ς. We consider a source at $r_0=0.8$, $\theta_0=0$ and two different axial positions; $x-x_0=0.5$ and $x-x_0=-0.5$. For the downstream Green's function we assume the contribution of the critical layer is small enough to ignore. In Figures 6 and 7 we plot the downstream and upstream Green's function contribution from each asymptotic eigenmode. The solid lines correspond to the real part of the Green's function and the dotted lines to the imaginary part, while the colours of the lines correspond to the impedances in Figure 4b. We also plot the numerical Green's function contribution in black.

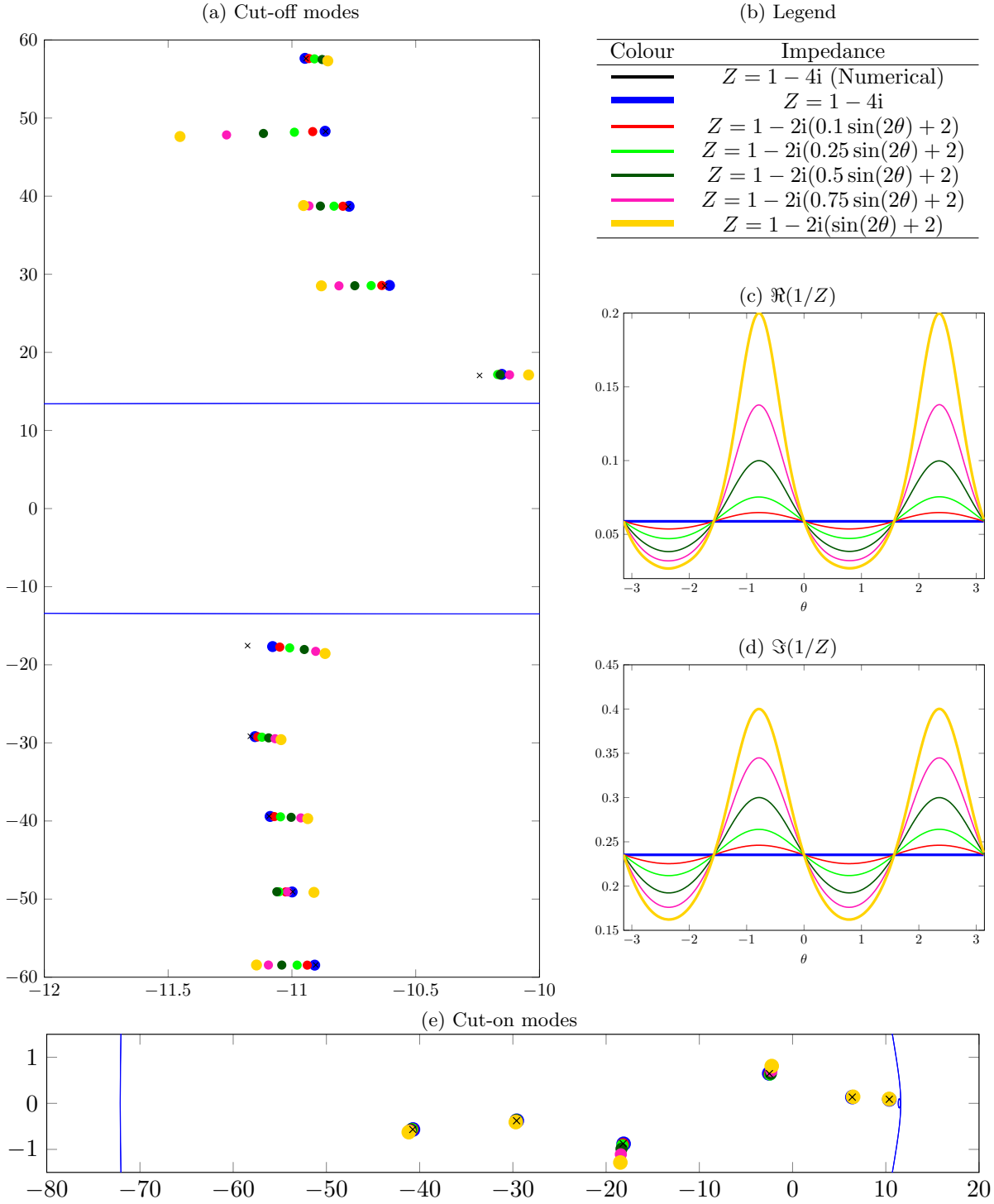

Figure 4: **Eigenmodes as lining varies circumferentially** We plot how the asymptotic eigenmodes vary as we consider different impedance functions, given in Figure 4b. We plot both the cut-on and cut-off modes. We plot the numerical eigenmodes when $Z = 1 - 4\mathrm{i}$ with black crosses. The mean flow is given by $U_x(r) = 0.2 + 0.4r^2$ and $U_\theta(r) = 0.1r + 0.2/r$ and the other parameters are $\omega = 25$, $n = 10$, $h = 0.6$ and $\theta_0 = 0$.

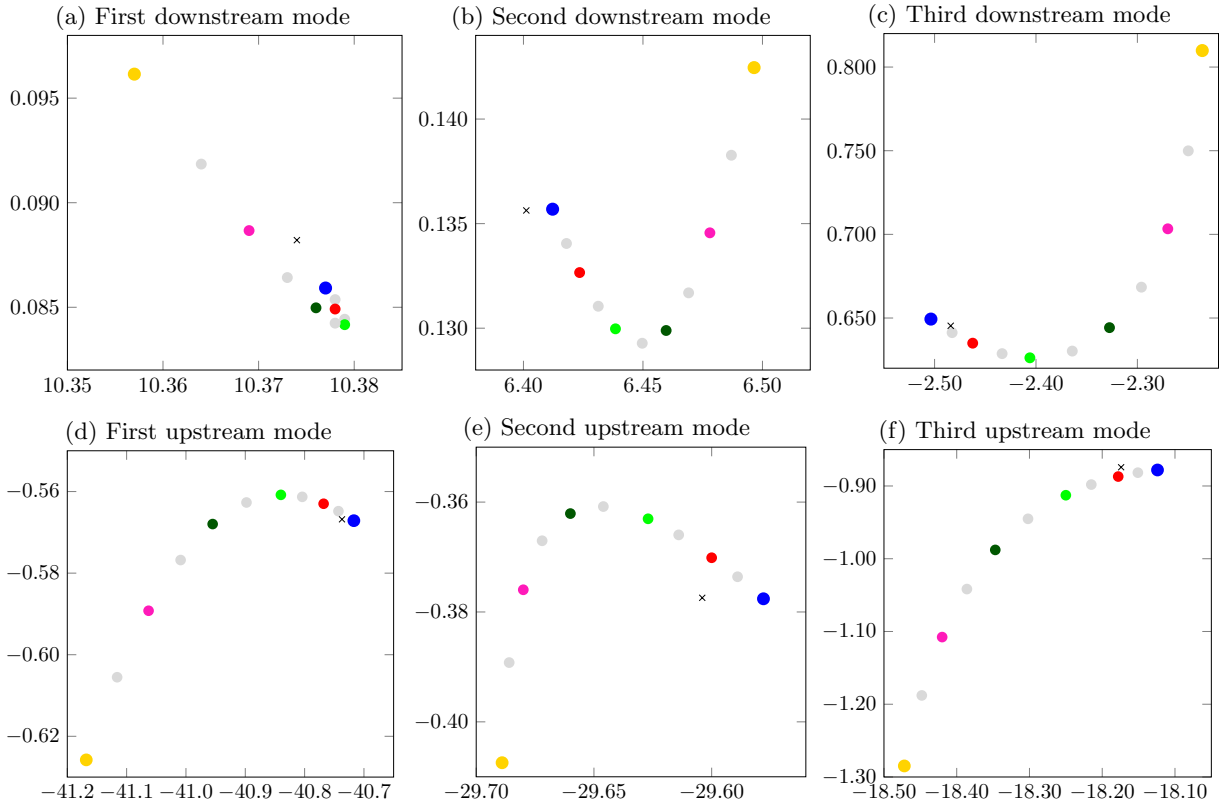

Figure 5: Close up of trajectories of eigenmodes from Figure 4 as we vary the impedance function Z^{ς}.

A. Upstream Green's function

In Figure 6 we plot the upstream asymptotic Green's function contribution from each asymptotic eigenmode. For the first upstream cut-on mode, numerically given by $k = -40.72 - 0.57\text{i}$, we see that the Green's function in Figure 6a hardly varies as we vary the impedance function. In Figure 6b we see the Green's function contribution from the second upstream cut-on mode, numerically given by $k = -29.58 - 0.38\text{i}$, varies a little more as we vary ς, but still not that much. The Green's function from the third upstream cut-on mode is in Figure 6c, and we see that while the real part of the Green's function is relatively unchanged, the imaginary part varies quite significantly.

The three cut-on eigenmodes are all a similar magnitude, with the cut-off eigenmodes a few orders of magnitude smaller. The total Green's function in Figure 6f thus comes from the summing the contribution from the three cut-on modes, and we see the imaginary part of the Green's function varying due to Figure 6c. In Figures 6d and 6e we see the Green's contribution from the first two cut-off modes. For the first cut-off mode, numerically given by $k = -11.08 - 17.67\text{i}$, we see the Green's function varies a small amount as we vary the impedance function, and it varies less in Figure 6e for the second cut-off mode. For subsequent cut-off modes we expect the Green's function to vary less and less as we vary the impedance function.

B. Downstream Green's function

In Figure 7 we plot the downstream asymptotic Green's function contribution from each asymptotic eigenmode. We see in Figure 7a that for the first downstream cut-on eigenmodes, numerically given by $k = 10.37 + 0.09\text{i}$ that the Green's function varies significantly as we vary the impedance function. However, only the imaginary part of the Green's function varies, with the real part staying relatively constant. In Figures 7b and 7c we see the contribution from the second and third downstream cut-on eigenmodes. For the second downstream eigenmode, both the real and imaginary part of the Green's function vary a small amount as ς varies, while for the third downstream eigenmode only the real part of the Green's function varies with impedance.

The total Green's function is now dominated by the second and third downstream cut-on eigenmodes, with

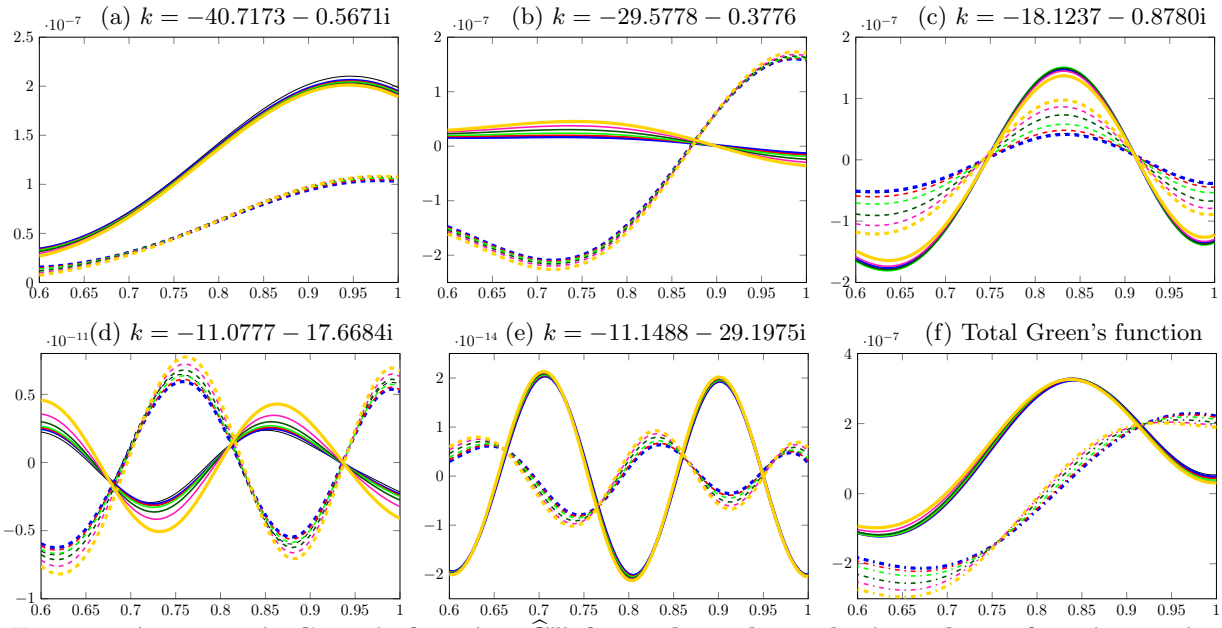

Figure 6: **Asymptotic Green's function $\widehat{G}_n^m$ for each mode as the impedance function varies when $n = 16$ with $x - x_0 = -0.5$ and $r_0 = 0.8$.** Solid lines correspond to the real part of the Green's function; dotted lines the imaginary part. The value of k in each figure refers to the numerical eigenmode when $Z = 1 - 4\mathrm{i}$. The numerical Green's function when $Z = 1 - 4\mathrm{i}$ is in black. The colours of the lines correspond to the impedances in Figure 4b. The other parameters are given in Figure 4.

the Green's function from the first upstream cut-on eigenmode one order of magnitude smaller, and the cut-off eigenmodes several orders of magnitude smaller. We see that the total Green's function varies moderately as we vary the impedance function, and varies by more than the downstream Green's function, due to the fact that the downstream eigenmodes vary more than the downstream eigenmodes. The Green's function from the first downstream cut-off mode in Figure 7d varies quite significantly as we vary the impedance function, with the Green's function varying significantly less in Figure 7e for the second downstream cut-off mode. As with the downstream Green's function, we expect the Green's function from subsequent downstream cut-off

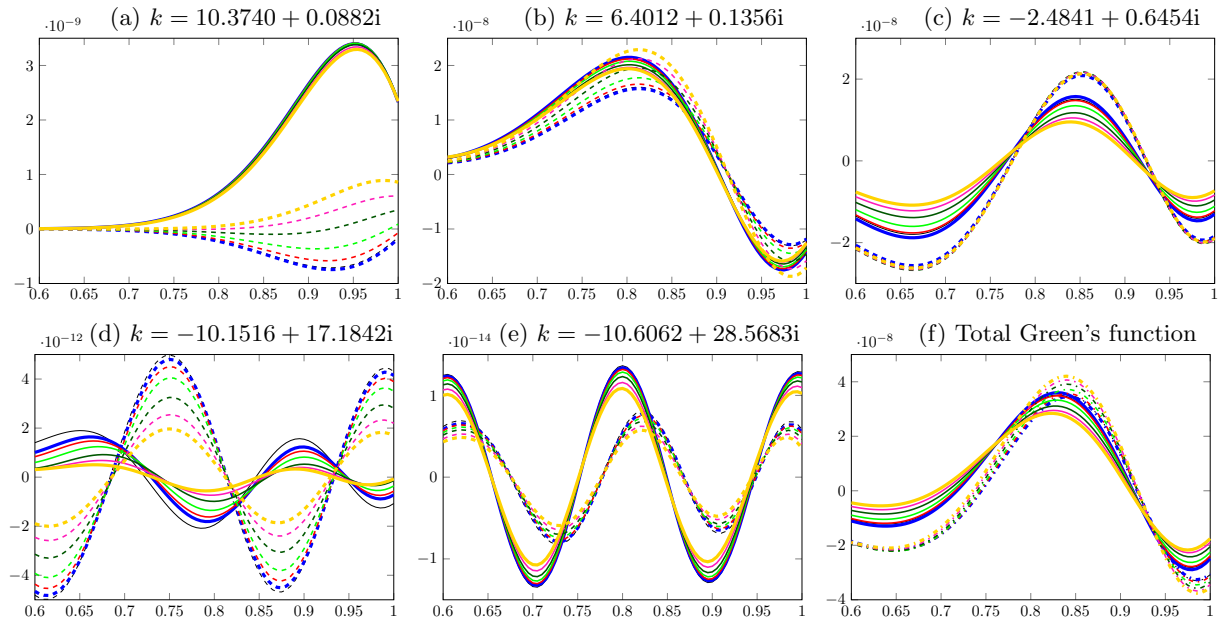

Figure 7: Same as Figure 6 but with $x - x_0 = 0.5$

modes to vary less and less as we vary the impedance function.

VII. Conclusion

In this paper we developed a new analytical method for calculating the eigenmodes and Green's function for swirling flow when the impedance of the acoustic lining varies circumferentially. This work has particular applications to splices in the acoustic lining, although we were not able to compute any results with spliced liners due to the computation time, and instead only considered a lining smoothly varying circumferentially. The acoustic analogy remains unchanged from Posson & Peake,[4] but the boundary conditions couple together all of the azimuthal modes. The analytical method involved taking a high-frequency limit and using the WKB method, as in Mathews & Peake.[2] The analytical dispersion relation for the eigenmodes is given by (43), and involves solving two infinite matrix problems numerically. These infinite matrix problems can be approximated by finite systems. The size of the matrices depends on the number of Fourier coefficients needed to accurately approximate the impedance by a truncated Fourier series, which is very large for a spliced liner since the impedance is a discontinuous function. In terms of a numerical solution, two methods were discussed in Mathews,[17] but both were unable to be implemented due to computation time.

We showed the the smoothly varying lining has a small effect on the acoustic eigenmodes, with some modes moving more than others. Of particular relevance is the fact that some of the modes with a small imaginary part can become more or less cut-on as we vary the impedance. To calculate the Green's function we evaluated the residue at each acoustic mode in the same way as in Mathews & Peake,[2] and ignored the critical layer contribution. In Figures 6 and 7 we plotted the Green's function for swirling mean flow at a downstream and an upstream axial source. We saw that the Green's function contribution for each acoustic mode generally varied only a small amount as we varied the lining, but for some modes the effect was quite significant. However, for this particular choice of parameters, when we sum up the contributions to get the total Green's function we found the Green's function only varied a small amount with the lining.

One possible future direction for research is investigating a fast method to solve for the eigenmodes and Green's function numerically when the lining varies circumferentially. Another method is revisiting the asymptotic method for finding the eigenmodes when the lining consists of splices, both in terms of how we can overcome Gibb's phenomena in representing the splice as a Fourier series and implementation speed. A final direction is to look at axial splices, although this problem would be much more suited to using the method of Weiner-Hopf.

Acknowledgments

This work was performed while James Mathews was still a Ph.D student (and makes up the majority of Chapter 5 in Mathews[17]) under the supervision of Professor Nigel Peake, and was supported by the UK Engineering and Physical Sciences Research Council (EPSRC) grant EP/H023348/1 for the University of Cambridge Centre for Doctoral Training, the Cambridge Centre for Analysis.

References

[1]Bender, C. M. and Orszag, S. A., *Advanced mathematical methods for scientists and engineers I: Asymptotic methods and perturbation theory*, Springer, 1978.

[2]Mathews, J. R. and Peake, N., "The acoustic Green's function for swirling flow in a lined duct," *Journal of Sound and Vibration*, Vol. 395, 2017, pp. 294–316.

[3]Posson, H. and Peake, N., "Swirling mean flow effect on fan-trailing edge broadband noise in a lined annular duct," *19th AIAA/CEAS Aeroacoustics Conference, Berlin*, 2013.

[4]Posson, H. and Peake, N., "The acoustic analogy in an annular duct with swirling mean flow," *Journal of Fluid Mechanics*, Vol. 726, 2013, pp. 439–475.

[5]Sijtsma, P., "Using phased array beamforming to locate broadband noise sources inside a turbofan engine," *AARC Engine Noise Phased Array Workshop, Cambridge (MA)*, 2006.

[6]Fuller, C. R., "Propagation and radiation of sound from flanged circular ducts with circumferentially varying wall admittances, I: Semi-infinite ducts," *Journal of Sound and Vibration*, Vol. 93, No. 3, 1984, pp. 321–340.

[7]Campos, L. M. and Oliveira, J. M., "On the acoustic modes in a cylindrical duct with an arbitrary wall impedance distribution," *The Journal of the Acoustical Society of America*, Vol. 116, No. 6, 2004, pp. 3336–3347.

[8]Brambley, E. J., Davis, A. M., and Peake, N., "Eigenmodes of lined flow ducts with rigid splices," *Journal of Fluid Mechanics*, Vol. 690, 2012, pp. 399–425.

[9]Wright, M., "Hybrid analytical/numerical method for mode scattering in azimuthally non-uniform ducts," *Journal of Sound and Vibration*, Vol. 292, No. 3, 2006, pp. 583–594.

[10]Pagneux, V., Amir, N., and Kergomard, J., "A study of wave propagation in varying cross-section waveguides by modal decomposition. Part I. Theory and validation," *The Journal of the Acoustical Society of America*, Vol. 100, No. 4, 1996, pp. 2034–2048.

[11]Bi, W., Pagneux, V., Lafarge, D., and Aurégan, Y., "Modelling of sound propagation in a non-uniform lined duct using a multi-modal propagation method," *Journal of Sound and Vibration*, Vol. 289, No. 4, 2006, pp. 1091–1111.

[12]Bi, W., "Calculations of modes in circumferentially nonuniform lined ducts," *The Journal of the Acoustical Society of America*, Vol. 123, No. 5, 2008, pp. 2603–2612.

[13]Mustafi, P., Astley, R. J., Sugimoto, R., and Kempton, A. J., "Acoustic Effects of Liner Damage on Zero-Splice Turbofan Intake Liners: Computational Study," *AIAA Journal*, Vol. 53, No. 3, 2014, pp. 703–712.

[14]Ingard, U., "Influence of fluid motion past a plane boundary on sound reflection, absorption, and transmission," *The Journal of the Acoustical Society of America*, Vol. 31, No. 7, 1959, pp. 1035–1036.

[15]Myers, M., "On the acoustic boundary condition in the presence of flow," *Journal of Sound and Vibration*, Vol. 71, No. 3, 1980, pp. 429–434.

[16]Masson, V., Mathews, J. R., Sanjose, M., Moreau, S., and Posson, H., "Liner behavior in an annular duct with swirling and sheared mean flow," *23rd AIAA/CEAS Aeroacoustics Conference, Denver*, 2017.

[17]Mathews, J. R., *Mathematical modelling of noise generation in turbofan aeroengines using Green's functions*, Ph.D. thesis, University of Cambridge, 2016.

[18]Boyce, W. E., DiPrima, R. C., and Haines, C. W., *Elementary differential equations and boundary value problems*, Wiley New York, 7th ed., 1992.